Journal of Applied Polymer Science

Crystallinity Evolution of Soft Segments During the Synthesis of Polyester-Based Waterborne Polyurethane

Gaohua Cao, Zhengbin Xia, Liang Lei, Yanhong Zhang, Junheng Xing
School of Chemistry and Chemical Engineering, South China University of Technology, Guangzhou, Guangdong 510640, China
Correspondence to: Z. Xia (E-mail: cezhbxia@scut.edu.cn)

ABSTRACT: Polyester-based waterborne polyurethane (WPU) dispersions having poly(ethylene glycol) adipate diol, isophorone diisocyanate, and hexamethylene diisocyanate as the main raw materials were synthesized by an acetone process. In each step of the synthesis process, the intermediate products were collected, and the crystallization morphologies and relative crystallinity (X) of the soft segments (SSs) in their films were investigated by means of polarizing optical microscopy, differential scanning calorimetry, and X-ray diffraction. The fracture surfaces and thermostability of the intermediate films were also investigated by scanning electron microscopy (SEM) and TGA, respectively. The results show that the crystalline dimensions of the SSs decreased substantially during the synthesis process of WPU. X of the SSs decreased after the prepolymerization reaction and increased after the hydrophilic chain-extending reaction, then decreased after emulsification, and finally increased after the secondary chain-extending reaction. Moreover, The SEM photos indicate that with decreasing crystalline dimensions, the fracture mechanisms of the intermediate films varied gradually from brittle failure to ductile fracture. The thermostability of the intermediates obtained in each step of the synthesis process was in accordance with the variation tendency of the X of the SSs. © 2013 Wiley Periodicals, Inc. J. Appl. Polym. Sci. **2014**, *131*, 40270.

KEYWORDS: crystallization; polyurethanes; structure–property relations; thermogravimetric analysis (TGA)

Received 24 July 2013; accepted 7 December 2013
DOI: 10.1002/app.40270

INTRODUCTION

Waterborne polyurethanes (WPUs) are an important group of materials that have been widely used in environmental coatings, adhesives, inks, and intelligent materials because of their outstanding mechanical properties, adhesive properties, and shape-memory functions.[1–4] In general, polyurethanes (PUs) can be treated as segmented polymers that consist of hard segments (HSs) and soft segments (SSs). Because of the thermodynamic noncompatibility of the SSs and HSs, microphase separation domains are often generated from the gathering of SSs and HSs, respectively. The degree of microphase separation largely affects the crystallization of PU. As a special condensed state, the crystallization of PU plays an important role on properties of its films. In the past few decades, the effects on crystallization of PU have been reported by many researchers.[5–9] The composition and structure of SSs, HSs, and ionic groups can affect the crystallization of PU. Fernández et al.[10] studied the effects of the parity of the number of methylenes of SSs on the crystallization of PU and found that the crystallizability of PU increased with the flexibility of the molecular chain; in addition, both the melting temperatures (T_m's) of the samples (from nonisothermal crystallization) and the equilibrium T_m's (from isothermal crystallization) changed with the number of methylenes according to a zig-zag plot characteristic of odd–even effect. Prisacariu and Scortanu[6] prepared two segmented PUs based on two isocyanates with different geometries: a flexible 4,4-dibenzyl diisocyanate and a conventional 4,4-methylene bis(phenyl isocyanate) with a rigid geometry. They found that the conformational mobility of 4,4-dibenzyl diisocyanate caused pronounced phase separation into a domain–matrix morphology and a higher tendency to crystallize and self-associate by hydrogen bonding. Zhu et al.[8] investigated the effects of ionic groups (—COO^-) on the crystallization and melting behavior of segmented PU ionomers. They concluded that the Coulombic forces between ionic groups within HS could affect the crystallization rate and crystal size of the SSs. In all, both HSs and SSs affected the crystallization and crystallinity of PU. For the crystallinity of PU having the same kinds of SSs, the contents and kinds of HSs were the main influencing factors. By contrast, in the crystallinity of PU with equal contents of HSs, the condensed state of the SSs, the strength of molecular polarity, the length of molecular chain, and the ion groups in the molecular chain can be crucial influencing factors.

For the sake of the specific performances or functions of PU products, many researchers have placed emphasis on the study of the influences of raw materials on the crystallization of PU.

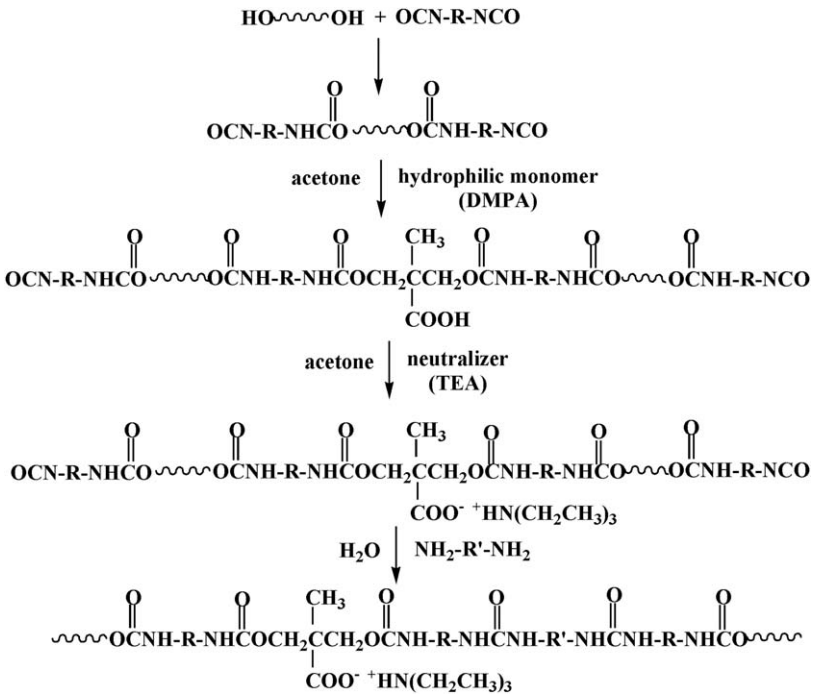

Figure 1. General steps of the WPU synthesis by the AT method.

However, the crystallinity evolution of SSs in the process of synthesizing WPU have rarely been reported. In fact, the synthesis method has a major impact on the properties of WPU. As is known, the acetone (AT) method is the most available method for WPU production in industry. Generally, the synthesis process of WPU by the AT method can be divided into three or four steps, as shown in Figure 1. However, poor repeatability of the AT method in preparing WPU occurs frequently because of a large number of variables in its preparation. In general, the intermediates and synthesis process are certain to affect the crystallization of the PU products; for instance, one can adjust the crystallinity of the prepolymer by controlling the reaction time and degree of prepolymerization. Therefore, explorations into the crystallinity evolutions of SSs in the process of synthesizing WPU are very important for the design and control of the crystallization of PU products.

According to the used polyols, WPU can be classified as a polyester-based or polyether-based PU. Generally, polyester-based PUs have better mechanical properties and higher crystallinities. For polyester-based PU materials, the crystallization behavior of the SSs has the greatest effects on the properties of the PUs, especially for PU materials with high SS contents. The crystallinity of the SSs of PUs has an important effect on their mechanical properties and heat resistance. Some PU intelligent materials, such as solid–solid phase-change PU materials and shape-memory PU materials, are also based on the crystallization of the SSs.[11,12]

In this study, sulfonate polyester based WPU dispersions with poly(ethylene glycol) adipate diol (PBA) as the SS and isophorone diisocyanate (IPDI), hexamethylene diisocyanate (HDI), *N*-(2-aminoethyl)-amino ethane sulfonated sodium (AAS), and ethane diamine (EDA) as the HSs were synthesized. The crystallization morphologies and relative crystallinity (X) of the SSs of the intermediate films of each completed step in the process of synthesizing WPU were investigated. The differences in the crystallization behaviors between the PU ionomers and nonionomers were compared through the introduction of AAS and *N*-ethyl ethylene diamine (NEED), whose molecular formulas were (1) AAS: $H_2N{-}CH_2{-}CH_2{-}NH{-}CH_2{-}CH_2{-}SO_3Na$ and (2) NEED: $H_2N{-}CH_2{-}CH_2{-}NH{-}CH_2{-}CH_3$. Furthermore, the fracture mechanisms of the products were studied, and the thermostability of the products were also evaluated.

EXPERIMENTAL

Materials

IPDI and HDI were purchased from Mitsubishi Chemical Industries (Tokyo, Japan) and were distilled before use. PBA (weight-average molecular weight = 3000 ± 50) and AT were industrial grade and were supplied by YangGuang Resin (Dongguan, China). AAS was reagent grade and was supplied by USI Corp. (Taiwan, China). NEED was reagent grade and was purchased from Tokyo Chemical Industry (Tokyo, Japan). EDA was reagent grade and was purchased from Lingfeng Chemicals (Shanghai, China).

Synthesis of the Samples

The AT method was used to synthesize polyester-based WPU, and the preparation process is illustrated in Scheme 1. In each step of the process, samples S1, S2, S3, S4, S5, and S6 were obtained, and the parameters of these samples are listed in Table I.

Prepolymerization. Amounts of 352 g of PBA (S1), 12 g of IPDI, and 26 g of HDI were added to a 2000-mL, four-necked flask with a condenser, thermometer, mechanical stirrer, and nitrogen tube. The reaction was carried out at 80°C for 3 h under a nitrogen atmosphere. Subsequently, the system was

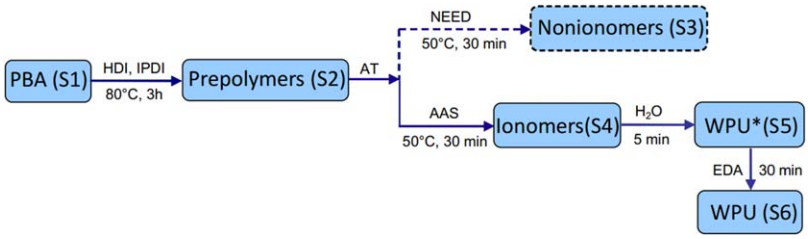

Scheme 1. Schematic illustration of the preparation process of the intermediates and WPU. [Color figure can be viewed in the online issue, which is available at wileyonlinelibrary.com.]

cooled to 60°C, and 400 g of AT was added to the stirring system. Then, the prepolymer (S2) solution was divided into two parts (systems A and B).

Primary Chain-Extending Reaction. Identical amounts of AT solution of NEED (3.7 g) and AAS (8 g) were add to the aforementioned A and B systems, respectively. Then, both the A system and the B system were kept stirring to react at 50°C for 30 min, and the nonionomers (S3) and ionomers (S4) were obtained.

Emulsification. Ionomers from step 2 were emulsified by 180 g of deionized water under high-speed shearing (5000 rpm) for 5 min, and the non-chain-extended waterborne polyurethane dispersion (WPU*, S5) was obtained.

Secondary Chain-Extending Reaction. WPU dispersions from step 3 were reacted with 0.95 g of EDA for 30 min, and then, the AT was removed from the obtained WPU dispersions by a rotary evaporator. Finally, the WPU dispersion (S6) with about 50% solid content was obtained.

Measurements

The samples (S1∼S6) were cast onto a Teflon plate at 60°C for 24 h. Then, the remaining solvent or moisture was removed at 50°C in a vacuum-drying oven for 48 h. Finally, the dry films were obtained and used for differential scanning calorimetry (DSC), X-ray diffraction (XRD), thermogravimetry (TG), and scanning electron microscopy (SEM) characterization.

The functional groups of the samples were measured by Fourier transform infrared (FTIR) spectroscopy (Spectrum2200, PerkinElmer). The samples were coated onto tin plates to obtain thin films at 60°C in vacuum-drying oven for 24 h, then cooled to 25°C, and tested.

The thermal properties of the samples were measured by differential scanning calorimetry (DSC; Q20, TA Instruments). To ensure a consistent thermal history for the melting process, samples of 5 mg each in alumina crucible were heated to 150°C and kept at that temperature for 3 min. After that, they were cooled to −30°C at a cooling rate of 10°C/min and then heated to 150°C at a rate of 10°C/min under a nitrogen atmosphere. The samples (S1–S6) for DSC, XRD, and TGA were collected after each corresponding step in the process of synthesizing of WPU and cast onto a Teflon plate at 60°C for 24 h. The remaining solvent or moisture was removed at 50°C in vacuum-drying oven for 48 h.

The crystallinity of the samples was measured by XRD (D8 Advance, Bruker, Germany). The scanning step was 0.02°, the scanning speed was 0.1 s/step, and the scanning angle was 10–60°.

The fracture surface morphologies of the samples were observed by SEM (S-3700N, Hitachi, Japan) with an acceleration voltage of 10 keV. The sample films were kept in a liquid nitrogen subcooler for 10 min and were then broken off. The fracture surface was jetted with gold and observed by SEM.

The thermostabilities of the samples were evaluated by thermogravimetric analysis (TGA; 2050, TA Instruments). Samples of 5 mg each in an alumina crucible were heated from 30 to 600°C at a heating rate of 10°C/min under a nitrogen atmosphere.

The crystallization morphologies of the samples were observed by polarizing optical microscopy (POM; XPL-2, Jiangnan Optics, China). The samples (S1–S4) for POM were collected and diluted to 0.5 wt % by AT after each corresponding step in the process of synthesizing WPU and were then dropped onto glass slides. The samples (S5 and S6) were collected and diluted to 0.5 wt % by deionized water and were then dropped onto the glass slides. All of samples (S1–S6) on glass slides were disposed of at 60°C for 24 h.

RESULTS AND DISCUSSION

FTIR Analysis

As shown in Figure 2, the peak at 3530–3540 cm^{-1} belonged to —OH groups in PBA (S1), whereas the peak area disappeared in S2–S6; this indicated that all of —OH groups were involved in the polymerization reaction. It was reported in the literature[8] reported that N—H groups free from hydrogen bonding had a stretching vibration at about 3450 cm^{-1}. However, the groups involved in hydrogen bonding had lower frequencies ranging from 3300 to 3200 cm^{-1}. The stretching vibrations of the N—H groups of all of the samples except S1 appeared from 3337 to 3382 cm^{-1}. This implied that parts of the N—H groups were

Table I. Formulation of the Intermediates and WPU

Sample	SSs content (%)	Ionic groups (mmol/g of resin)	Solvent
PBA (S1)	100	0	AT
Prepolymers (S2)	90.37	0	AT
Nonionomers (S3)	89.60	0	AT
Ionomers (S4)	88.74	0.19	AT
WPU* (S5)	88.74	0.19	Water
WPU (S6)	88.34	0.19	Water

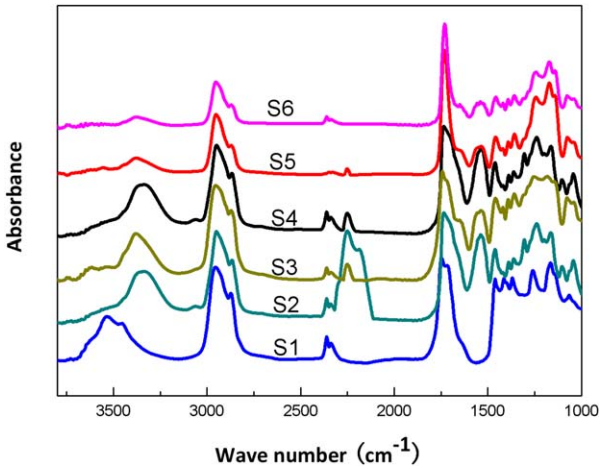

Figure 2. FTIR spectra of the PBA (S1), prepolymers (S2), nonionomers (S3), ionomers (S4), WPU* (S5), and WPU (S6). [Color figure can be viewed in the online issue, which is available at wileyonlinelibrary.com.]

involved in hydrogen bonding. The peak area at 2280–2240 cm^{-1} belonged to the —NCO groups of S2–S5, as shown in Figure 2. The peak intensity of the —NCO groups decreased obviously from S2 to S5 and disappeared in S6; this suggested that the contents of —NCO decreased with the polymerization reaction. The peak area at 1730–1735 cm^{-1} belonged to the C═O groups of ester groups, which came from the ester groups of PBA and/or urethane, so it appeared in the curves of all of the samples. In addition, the area of 1640–1645 cm^{-1} was the peak area of the C═O groups in urea (produced from the reaction of —NCO and HN—); this illustrated that the urethane–urea structure was formed in S3–S6; in contrast, S2 had no peak at 1640–1645 cm^{-1} because it was synthesized by PBA (—OH) and isocyanates (—NCO). The peak at 1065 cm^{-1} belonged to the —SO_3Na groups, which were found in S4, S5, and S6 because of the introduction of AAS.

DSC Analysis

On the basis of the DSC data (Figure 3), the encircling area of the DSC curve and base line were converted into enthalpy [crystallization enthalpy (ΔH_c) and melting enthalpy (ΔH_m)], and the results are shown in Table II. The crystallization peak temperature and melting peak temperature in the DSC curves were defined as the crystallization temperature (T_c) and T_m, respectively.[13]

As shown in Figure 3, the crystallization peak of PBA (S1) was very sharp; this implied that it had the highest crystallization rate. Because the regularity of SS was broken up by HSs, X of prepolymers (S2) fell to 56.77%. In addition, T_c and T_m of S2 were also lower than those of S1; this indicated that the crystallizability of the SSs decreased. The relative crystallinity of the chain-extended products [nonionomers (S3) and ionomers (S4)] was enhanced compared with that of the prepolymers (S2); this suggested that a greater content HS would not always lead to a lower crystallinity of SS. In fact, S3 and S4, having longer PU chains and many more urea groups after the chain-extending reactions, could make their HSs stack together compactly and improve the relative crystallinity of their SSs.

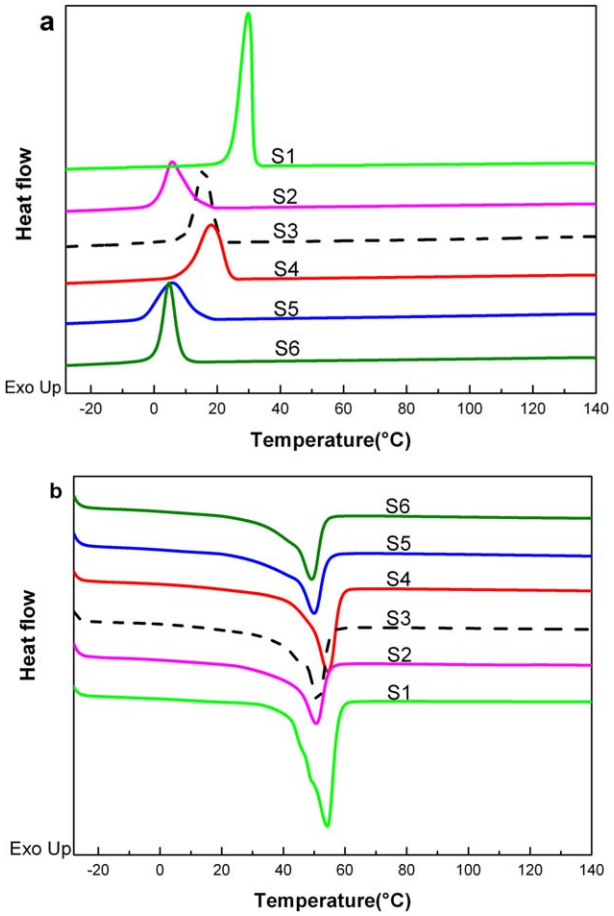

Figure 3. DSC curves of PBA (S1), prepolymers (S2), nonionomers (S3), ionomers (S4), WPU* (S5), and WPU (S6): (a) cooling scans and (b) second heating scans. [Color figure can be viewed in the online issue, which is available at wileyonlinelibrary.com.]

Moreover, the differences in the relative crystallinity between S3 and S4 indicated that the sulfo group improved the relative crystallinity of the SSs by increasing the degree of microsphere separation of the SSs and HSs.

Emulsification is a necessary step in the preparation of WPU dispersions. As shown in Table II, X of WPU* (S5) was lower than that of the ionomers (S4). During the emulsification and drying process, residual —NCO groups in the ionomers could

Table II. Relevant Data of the DSC Curves of the PBA (S1), Prepolymers (S2), Nonionomers (S3), Ionomers (S4), WPU* (S5), and WPU (S6)

Sample	T_c (°C)	ΔH_c (J/g)	T_m (°C)	ΔH_m (J/g)	X (%)[a]
S1	29.82	56.35	54.33	56.36	100
S2	5.99	31.99	50.89	31.95	56.77
S3	16.07	37.05	51.23	37.49	65.75
S4	18.31	40.15	54.63	40.21	71.25
S5	5.74	32.11	49.25	32.79	56.98
S6	5.80	33.10	50.51	33.41	58.74

[a] $X = \Delta H_c/\Delta H_{co} \times 100\%$, where ΔH_{co} is the crystallization enthalpy of PBA and ΔH_c is the crystallization enthalpy of the other samples.

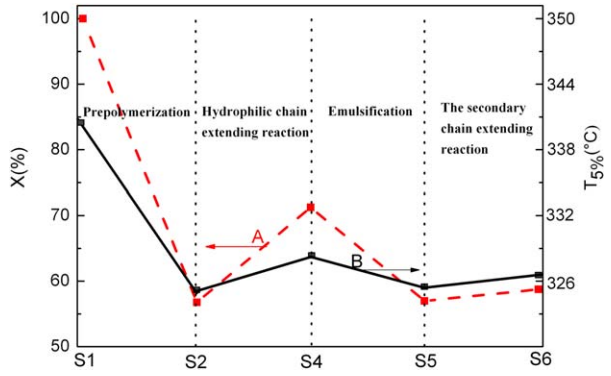

Figure 4. (A) Variation tendency of *X* of the SSs in the process of the WPU synthesis and (B) $T_{5\%}$ of the PBA (S1), prepolymers (S2), ionomers (S4), WPU* (S5), and WPU (S6). [Color figure can be viewed in the online issue, which is available at wileyonlinelibrary.com.]

react with H_2O and increase the content of HSs; this decreased *X* of S4 to some extent. More importantly, the solvents of S4 and S5 were AT and water, respectively. The different solvents caused different condensed states of the PU molecular chain; this was the major reason for difference in *X* between S4 and S5. Further discussion is included in the POM graph analysis.

X of S6 was slightly enhanced compared with that of S5 as a result of the generation of urea with strong polarity and the elongation of the molecular chain in the secondary chain-extending reaction.

In brief, the DSC results indicated that the *X* of SS decreased after the prepolymerization reaction and increased after the hydrophilic chain-extending reaction. It then decreased after emulsification and increased after the secondary chain-extending reaction. The variation tendency of the *X* of the SSs during the synthesis of WPU is shown in Figure 4(A).

XRD Analysis

The typical wide-angle XRD pattern of PU consists of a sharp diffraction peak below 4.5° (2θ), and three to four peaks appear in the 2θ region from 10 to 30°.[14]

The XRD patterns of the samples are shown in Figure 5, where it is shown that all of the samples had two prominent peaks at Bragg angles of about 21.8 and 24.8°. This indicated that the crystalline structure stemmed from the SSs (PBA), if the minor mismatches of Bragg angles could be ignored. It is worth noting that the intensity of peaks weakened after the prepolymerization reaction, strengthened after the hydrophilic chain-extending reaction, then weakened after emulsification, and strengthened after the secondary chain-extending reaction. That is, the variation tendency of the crystallinity of samples in each step of the synthesis of WPU was in accordance with the *X* of the SSs. This also suggested that the crystallization of PU resulted from the crystallization of the SSs. In addition, as Figure 5 shows, the half-peak width also increased in the process of synthesizing WPU; this implied that the crystal size of the SSs became smaller.[15]

POM Graphical Analysis

Figure 6 shows the POM images of the PBA, prepolymers, nonionomers, ionomers, and WPU. We found that WPU* (S5) and WPU (S6) displayed the same crystallization morphology (i.e., the secondary chain-extending reaction had little influence on the crystallization morphology of the films), so we just included the POM graph of S5.

As shown in Figure 6, the films of the PBA [Figure 6(a,b)], prepolymers [Figure 6(c)], and ionomers [Figure 6(e)] presented obvious Maltese cross patterns, which were generated from the birefringent properties and radial optical symmetry of the polymer spherulites. Among them, the spherocrystal diameter of PBA was the largest (ca. 30 μm) because of its well-defined structure. In addition, a cobweblike crystallization morphology was found from PBA [Figure 6(b)], and to the best of our knowledge, the cobweblike crystallization morphology may have generated from the radial growth of the polymer spherulites.

As a result of the introduction of HSs and the destruction of the regularity of the SSs, the crystalline dimensions of the prepolymers (ca. 15 μm) decreased compared with those of PBA. The nonionomers [Figure 6(d)], obtained by the chain-extending reaction of NEED and the prepolymers, displayed a very irregular crystallization morphology. In contrast, the ionomers [Figure 6(e)], acquired by the chain-extending reaction of AAS and the prepolymers, still inherited the regular Maltese cross patterns of the prepolymers, except that its crystalline dimensions were smaller (ca. 8 μm). The differences in the crystallization morphologies between the nonionomers and ionomers suggested that the sulfo group within the HSs promoted the microphase separation of the SSs and HSs and also maintain the Maltese cross crystallization morphology of the SSs. As the POM graphs of the ionomers [Figure 6(e)] and WPU* [Figure 6(f)] show, the spherocrystals of the samples in AT were much larger than those in water. This illustrated that the solvent had an important effect on the crystalline dimensions of PU. The reason for this phenomenon was that the PU molecular chain in AT (as a good solvent for PU) could stretch freely; that is, the motion resistance was smaller for the PU molecular chain in AT than that in water; this led to the more perfect PU crystallization in AT. As shown in Figure 6(f), the crystallization of WPU was very small but intensive; this largely contributed

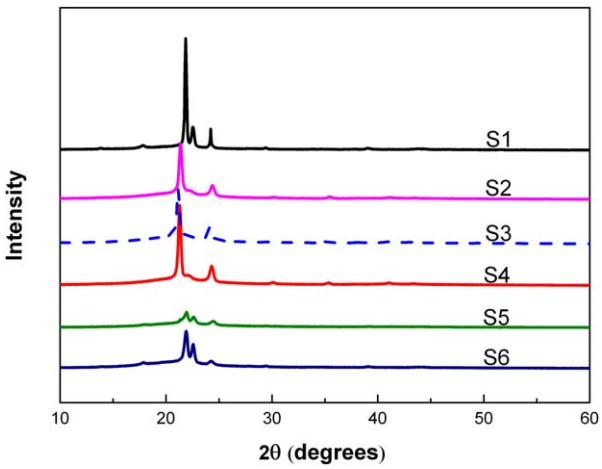

Figure 5. XRD profiles of the PBA (S1), prepolymers (S2), nonionomers (S3), ionomers (S4), WPU* (S5), and WPU (S6). [Color figure can be viewed in the online issue, which is available at wileyonlinelibrary.com.]

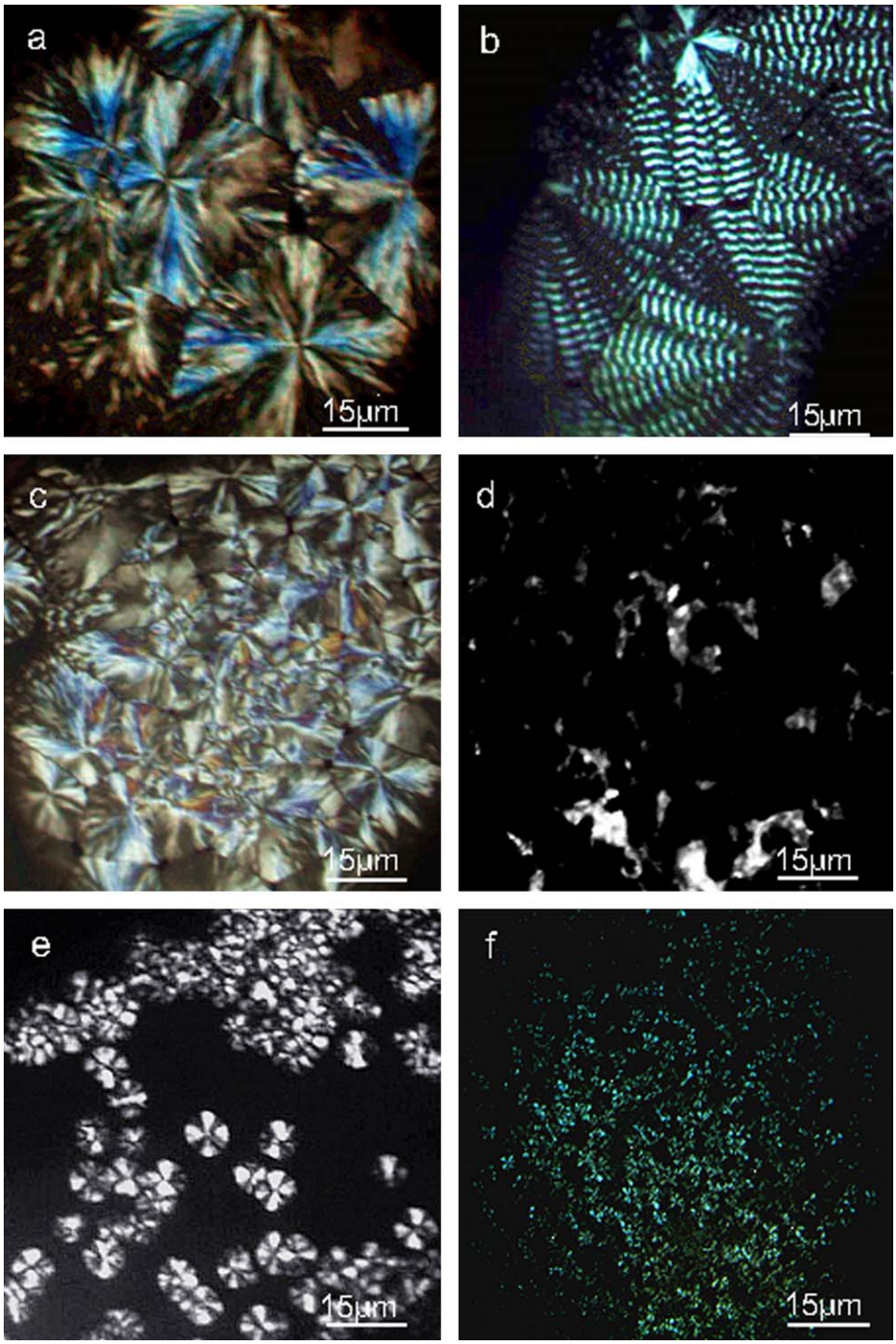

Figure 6. POM graphs of the (a,b) PBA, (c) prepolymers, (d) nonionomers, (e) ionomers, and (f) WPU. [Color figure can be viewed in the online issue, which is available at wileyonlinelibrary.com.]

to its excellent mechanical properties and adhesive strength. Briefly, the crystalline dimensions decreased substantially in the process of synthesizing WPU.

SEM Analysis

The SEM was used to detect the fracture surface morphologies of the samples. To the best of our knowledge, the cracks of the materials extended quickly when a brittle failure occurred; consequently, the fracture surface was relatively smooth. By contrast, the fracture surface of ductile fracture was intricate and misty because of the complicated fracture mechanisms and greater energy consumption.[16,17] As Figure 7(a) depicts, the white cracks of PBA were ridgelike on a large scale; this suggested that the large crystalline dimensions of PBA resulted in

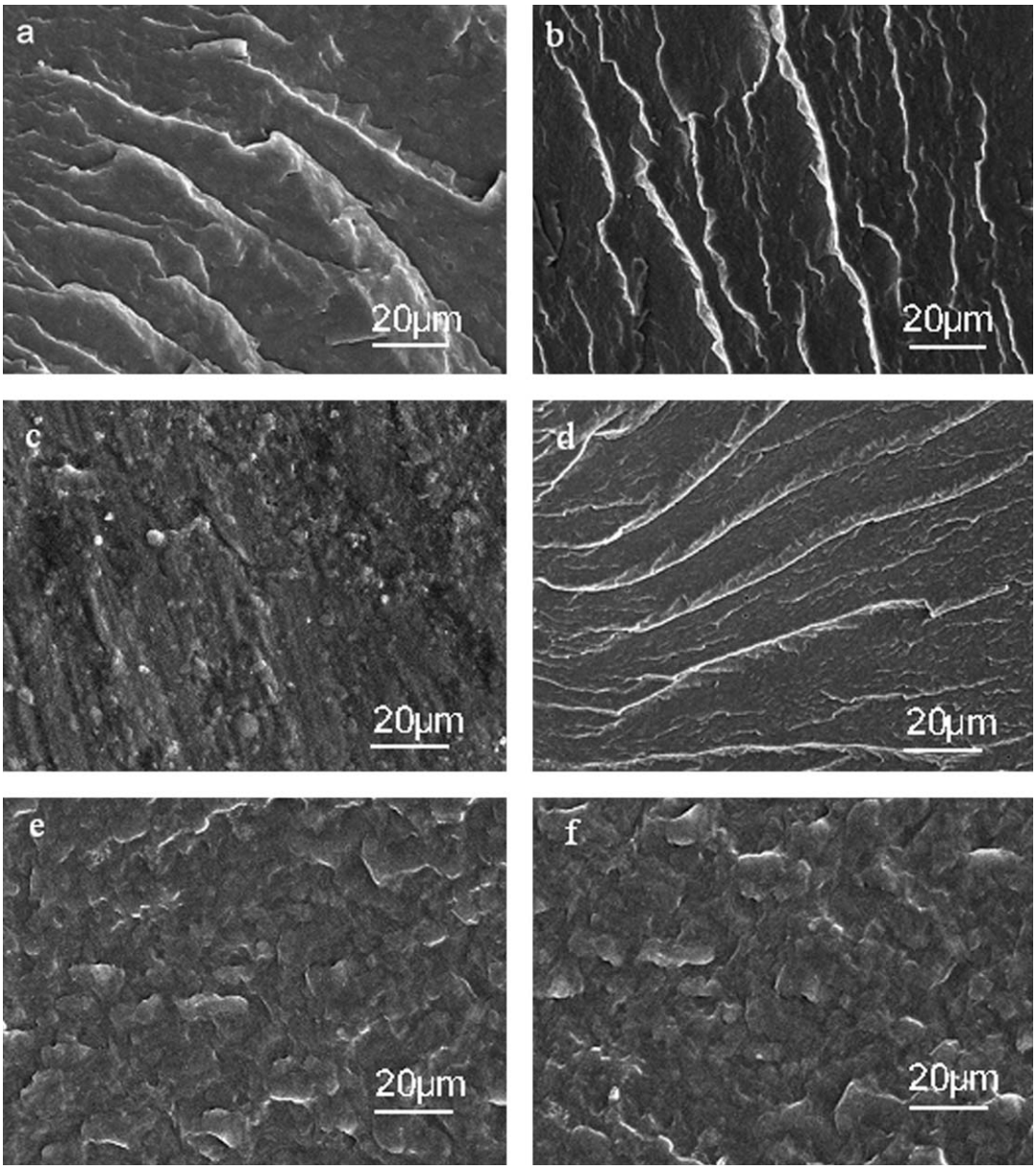

Figure 7. Fracture surface SEM photos of films of the (a) PBA, (b) prepolymers, (c) nonionomers, (d) ionomers, (e) WPU*, and (f) WPU.

brittle failure on the macroscopic level and its poor impact resistance and elasticity in the mechanical properties. With decreasing crystalline dimensions, the cracks of the prepolymers [Figure 7(b)] and ionomers [Figure 7(d)] became longer and narrower, especially for ionomers. White beardlike cracks appeared around the long cracks, and this implied that the flexibilities of the prepolymers and ionomers was better than that of PBA. Figure 7(c) shows a different fracture surface with sags and crests due to the irregular structure of the nonionomers. It is worth noting that the cracks of WPU were small and dispersive; this was totally different from that of the former. In other words, it was difficult to break the WPU film off, even at extremely low temperatures (in liquid nitrogen). The small but intensive crystal within WPU may have led to its excellent flexibility. In brief, with decreasing crystalline dimensions, the fracture mechanisms of the films varied gradually from brittle failure to ductile fracture.

TGA

Many researchers have studied the mechanisms and kinetics of the thermal decomposition of PU for the sake of improving its thermostability.[18–22] Normally, decomposition of HSs is the first step in the process of the thermal decomposition of PU because the decomposition temperatures of urethane, allophanate, and urea bonds within HS are much lower than that of SSs. Li et al.[23] studied the thermal decomposition of PU and found that the composition, structure, content, and distribution of HS had primary effects on the PU thermostability. Moreover, the amorphous regions in the HSs could be easily decomposed.

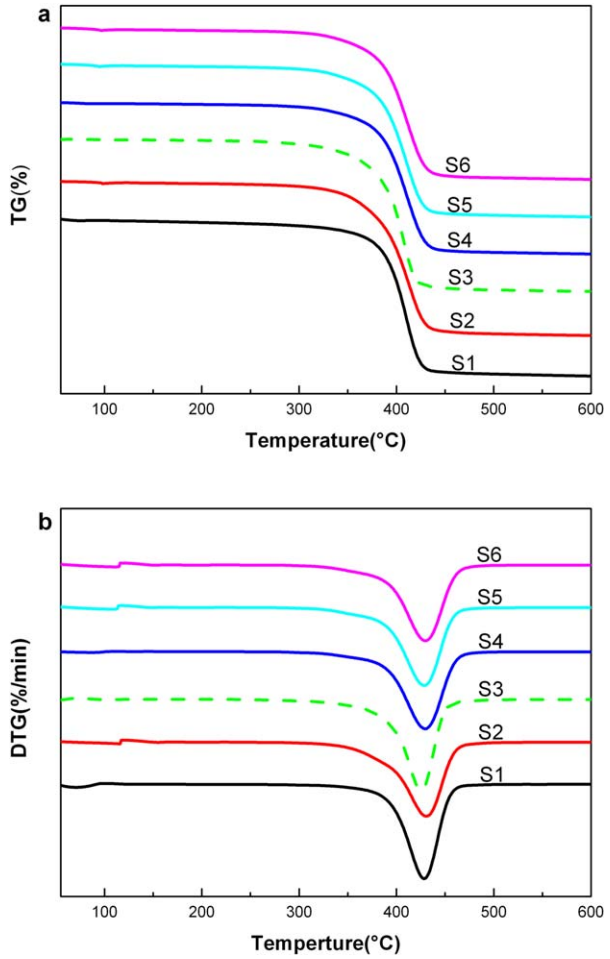

Figure 8. (a) TG and (b) DTG curves of the PBA (S1), prepolymers (S2), nonionomers (S3), ionomers (S4), WPU* (S5), and WPU (S6). [Color figure can be viewed in the online issue, which is available at wileyonlinelibrary.com.]

Figure 8 shows the TG and differential thermogravimetry (DTG) curves of the samples. Where $T_{x\%}$ represents the temperature at x % mass loss of the sample and T_{max} represents the temperature at the fastest decomposition rate of sample, the detailed data of the TG and DTG curves are listed in Table III. As shown in Figure 8 and Table III, the T_{max} values of the samples were about 410°C as a result of the high content of SSs in all of the samples. However, the $T_{5\%}$ values of the samples differed greatly. Among them, the $T_{5\%}$ of PBA (S1) was the highest. Compared with S1, the $T_{5\%}$ of S2 fell substantially because of the existence of HSs. As for the thermostability of S3, its $T_{5\%}$ fell 8.5°C compared with S2 as a result of the increase in HS content and the low degree of microsphere separation. By contrast, the $T_{5\%}$ of S4 rose 3.3°C compared with that of S2 because of the introduction of ion groups.

On the basis of the data of the X and $T_{5\%}$ values of the samples in Figure 4, we found that the variation tendency of the thermostability of the samples (S1, S2, S4, S5, and S6) was in accordance with the X values of the SSs in the steps of synthesizing WPU. This meant that the high X of the SSs promoted the aggregation of the HSs; as a result, the amount of amorphous regions within the HSs decreased, and this could improve the thermostability of the samples.

Table III. Relevant Data of TGA of the PBA (S1), Prepolymers (S2), Nonionomers (S3), Ionomers (S4), WPU* (S5), and WPU (S6)

Samples	$T_{5\%}$ (°C)	$T_{10\%}$ (°C)	$T_{50\%}$ (°C)	T_{max} (°C)
S1	340.1	351.7	403.4	410.9
S2	325.5	351.4	402.9	410.2
S3	317.0	348.0	400.3	408.0
S4	328.8	354.5	404.4	410.8
S5	325.9	351.6	402.7	409.7
S6	327.2	353.5	404.6	410.5

CONCLUSIONS

WPU was prepared by an AT method, and the intermediates were collected and studied during the synthesis process. The DSC results indicate that in the steps of synthesizing WPU, the X values of the SSs decreased after the prepolymerization reaction, increased after the hydrophilic chain-extending reaction, decreased after emulsification, and then increased after the secondary chain-extending reaction. The introduction of sulfo groups improved the degree of microsphere separation and the relative crystallinity of the SSs. The XRD results show that the crystallization of PU resulted from the crystallization of the SSs. The POM graphs reveal that the crystalline dimensions of the SSs decreased substantially during the process of synthesizing WPU. The differences in the crystallization morphologies between the nonionomers and ionomers suggested that the ionic group within the HSs promoted the microphase separation of the SSs and HSs. The crystals of PU in water were smaller and less perfect than those of PU in AT. The SEM photos demonstrated that during the process of synthesizing WPU, the fracture mechanisms of the films gradually varied from brittle failure to ductile fracture with decreasing crystalline dimension. The TGA results suggest that the high X of the SSs and the high degree of microsphere separation between the SSs and HSs improved the thermostability of the samples. What is more, the variation tendency of the thermostability of the samples was in accordance with the X of the SSs in the steps of synthesizing WPU. The crystallinity evolution of SS in the process of synthesizing WPU implied potential applications in the design and control of the crystallization of PU products through the control of the degree of prepolymerization and molecular chain length and the introduction of ion groups and strong polar groups.

REFERENCES

1. Erica, S.; Stefano, R.; Flavio, D.; Caterina, Z. *Prog. Org. Coat.* **2011**, *72*, 81.
2. Orgilés-Calpena, E.; Arán-Aís, F.; Torró-Palau, A. M.; Orgilés-Barceló, C. *J. Dispersion Sci. Technol.* **2012**, *33*, 147.
3. Chang, C. J.; Tzeng, H. Y. *Polym.* **2006**, *47*, 8536.

4. Lee, S. K.; Yoon, S. H.; Chung, I.; Hartwig, A.; Kim, B. K. *J. Polym. Sci. Part A: Polym. Chem.* **2011**, *49*, 634.
5. Mondal, S.; Hu, J. L. *Polym. Int.* **2006**, *55*, 1013.
6. Prisacariu, C.; Scortanu, E. *Macromol. Symp.* **2007**, *254*, 153.
7. Liu, J.; Ma, D. Z. *J. Appl. Polym. Sci.* **2002**, *84*, 2206.
8. Zhu, Y.; Hu, J. L.; Yeung, K. W.; Liu, Y. Q.; Liem, H. M. *J. Appl. Polym. Sci.* **2006**, *100*, 4603.
9. Kim, B. K.; Lee, J. S.; Baek, S. H.; Choi, Y. J.; Lee, J. O.; Xu, M.; Lee, S. Y. *Polym.* **1998**, *39*, 2803.
10. Fernández, C. E.; Bermudez, M.; Versteegen, R. M.; Meijer, E. W.; Muller, A. J.; Muñoz-Guerra, S. *J. Polym. Sci. Part B: Polym. Phys.* **2009**, *47*, 1368.
11. Cao, Q.; Liu, P. S. *Eur. Polym. J.* **2006**, *42*, 2931.
12. Jeong, H. M.; Ahn, B. K.; Cho, S. M.; Kim, B. K. *J. Polym. Sci. Part B: Polym. Phys.* **2000**, *38*, 3009.
13. Zhu, Y.; Hu, K. F.; Yaung, K. W.; Meng, Q.; Chen, S. *J. Appl. Polym. Sci.* **2008**, *107*, 599.
14. Ranganathan, T.; Gowd, E. B.; Ramesh, C.; Kumar, A. *J. Polym. Sci. Part A: Polym. Chem.* **2005**, *43*, 1903.
15. Chen, S. J.; Hu, J. L.; Liu, Y. Q. *Polym. Int.* **2007**, *56*, 1128.
16. Diamond, S.; Mindess, S. *Cement and Concrete Research.* **1992**, *22*, 67.
17. McDanels, D. L. *Metall. Trans. A.* **1985**, *16*, 1105.
18. Czech, Z.; Pelech, R. *Prog. Org. Coat.* **2010**, *67*, 72.
19. Rogaume, T.; Valencia, L. B.; Guillaume, E.; Richard, F.; Luche, J.; Rein, G.; Torero, J. L. *Combust. Sci. Technol.* **2011**, *183*, 627.
20. Foti, S.; Maravigna, P.; Montaudo, G. *J. Polym. Sci. Part A: Polym. Chem.* **1981**, *19*, 1679.
21. Bilbao, R.; Mastral, J. F.; Ceamanos, J.; Aldea, M. E. *J. Anal. Appl. Pyrolysis* **1996**, *37*, 69.
22. Endres, W.; Lechner, M. D.; Steinberger, R. *Macromol. Mater. Eng.* **2003**, *288*, 525.
23. Li, Y. J.; Gao, T.; Liu, J.; Linliu, K.; Desper, C. R.; Chu, B. *Macromolecules* **1992**, *35*, 7365.